Stereoscopic MicroPIV Measurements in A Labyrinth-Channel Dripper Used in Micro-Irrigation Systems

Gökhan Ergin, M Amielh, Séverine Tomas, Jafar Al-Muhammad, Jean-Jacques Lasserre, Fabien Anselmet

Stereoscopic MicroPIV Measurements in A Labyrinth-Channel Dripper Used in Micro-Irrigation Systems

Gökhan Ergin[1,*], Muriel Amielh[2], Severine Tomas[3], Jafar Al-Muhammad[2,3], Jean-Jacques Lasserre[4], Fabien Anselmet[2]
1: Dantec Dynamics, Skovlunde, Denmark
2: IRPHE, Marseille, France
3: IRSTEA, UMR G-EAU, Montpellier, France
4: Dantec Dynamics, Marseille, France

* Correspondent author: gokhan.ergin@dantecdynamics.com

Keywords: Micromixing, Drip irrigation, Stereoscopic Micro PIV, Microfluidics, Passive micromixer

ABSTRACT

Small serpentine-shaped channels used in drip irrigation is an efficient irrigation technique in order to spare water. Eventual clogging in such micro channels should be avoided to extend the lifetime of these irrigation systems. Clogging often occurs when sedimentation takes place in low or zero velocity regions in steady laminar flow conditions. For this reason, labyrinth dripper designs are used to enhance mixing and / or induce unsteady flow conditions inside the channel. The aim of the present study is to investigate the flow inside such millimetric complex channel geometry with Stereoscopic MicroPIV measurements. Current three-component (3C) velocity measurements are compared with previous two-component (2C) velocity measurements. Results indicate that the u and v components of the 3C measurements are in good agreement with the previous 2C measurements, identifying and confirming the previously measured low- and zero-velocity regions. Furthermore, the out-of-plane (w) velocity component adds new information about the flow field revealing three-dimensional (3D) flow structures, what appears to be oblique vortices emanating from the baffle tips. In conclusion, both enhanced mixing due to 3D vortices and induced unsteady flow field seems to be responsible for clogging suppression.

1. Introduction

There is a growing trend in agriculture towards more efficient irrigation systems, as water is becoming a scarce resource for human survival. According to the world resource institute (www.wri.org), the water stress is expected to increase substantially by 2040, due to increasing population, global warming, and increasing food demand (Figure 1). Today, agriculture accounts for 70% of freshwater withdrawals on average, with up to 90% in some developing countries. Unfortunately, 80% of irrigation is still performed using furrow irrigation, which is the oldest and least efficient irrigation technique. Sprinkler irrigation is more efficient with 17% and micro irrigation is the most efficient irrigation technique with only 3% usage worldwide. Despite their cost, there is a shift towards more efficient micro-irrigation techniques like drip irrigation.

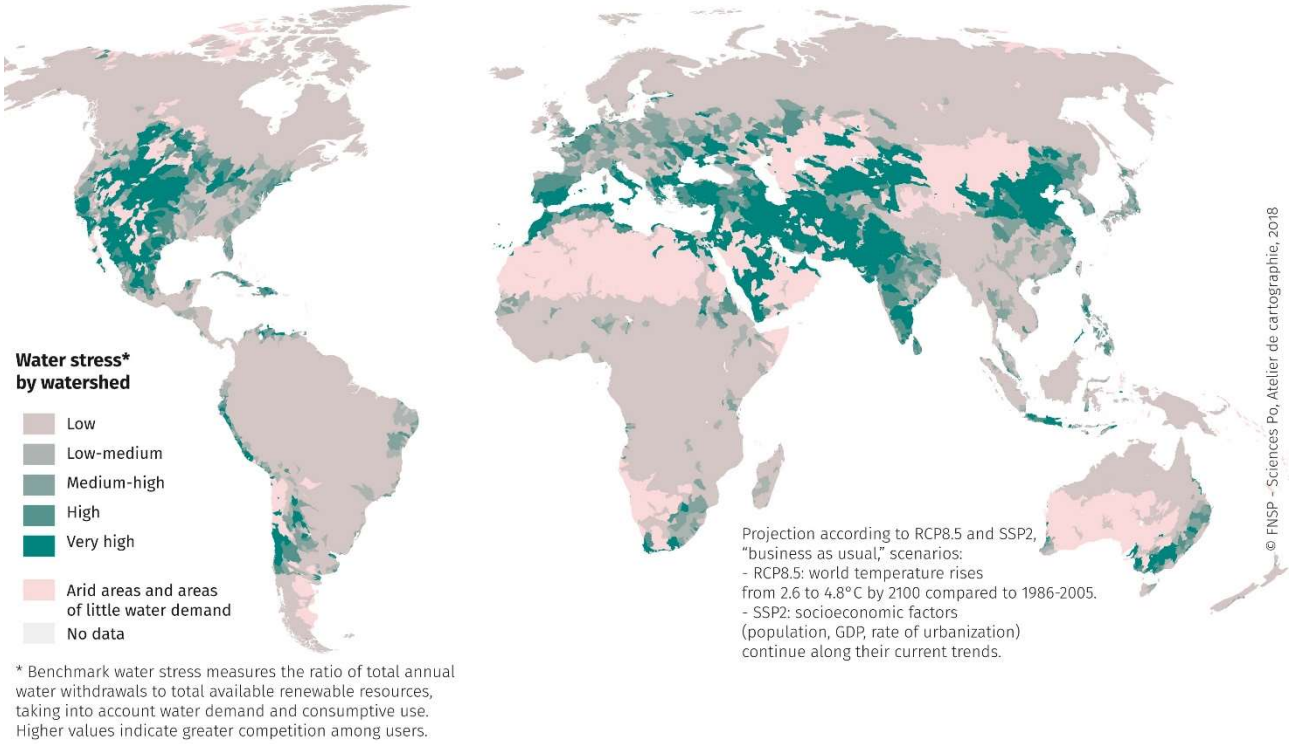

Fig. 1. Projected water stress in 2040. Source: World Resources Institute, www.wri.org

Low-cost drip irrigation nozzles are passive micromixer devices (Figure 2) which rely entirely on the fluid pumping energy with the least number of moving parts. In these devices, the channel geometry is the main design parameter that affects the durability. Often the irrigation nozzles have a channel topology (Figure 2) that introduces a large pressure drop to maintain the flow in an irrigation network. Choosing a small exit cross section could be one solution but, this approach often leads to clogging problems in the long term. This reduces the useful lifetime of the irrigation nozzle, which produces more plastic waste over time, and this has a negative impact both on the environment and on the farming cost.

The nominal flow rates and dimensions used in drip irrigation nozzles result in Reynolds numbers around 500, therefore clogging is promoted in regions with low or zero velocity for extended periods of time where particles get a chance for deposition on the channel walls. Extensive MicroPIV measurements have been performed to characterize the two-dimensional (2D) flow field for this microchannel (2,3), but the 3D flow field characterization was not considered. In Ref (3), some regions were identified as shear motion zone and vortex zones based on the 2D velocity data, i.e. only the mean vorticity in the z-direction was studied. However, serpentine micromixers with sharp turns are found to induce oblique vortices (4,5), and these could be responsible for enhanced mixing and reduced clogging in the irrigation nozzle. Furthermore, in Ref (2) and (3) the unsteady movement of the low- or zero-velocity regions were not considered. If these low- or zero-velocity zones move within the serpentine, i.e. if their position is not steady, the particles may not have sufficient time to settle in one position, which may be responsible for the delay of clogging. The aim of this study is :

- to compare the current three-component (3C) measurements with the 2C measurements in Ref (2),
- to identify any oblique vortices emanating from the baffle tips,
- to identify any low- and zero-velocity regions and investigate their steadiness,
- evaluate the results with respect to clogging considering the new information inferred from the Stereo MicroPIV measurements.

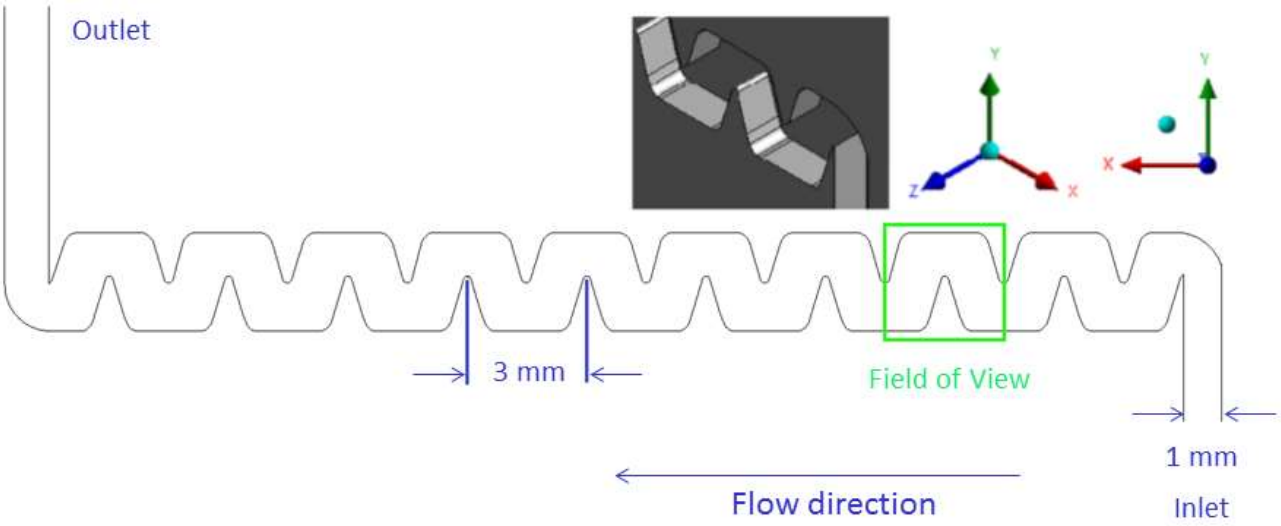

Fig. 2. Labyrinth channel flow geometry used in the experiments(1)

2. Stereoscopic MicroPIV

Experiments are performed using the Stereoscopic MicroPIV technique (Fig. 3a) as it can provide the necessary multiple-component velocity information in the investigated irrigation serpentine with micron scale resolution. All three velocity components are measured in the center height of the microchannel, around the 3rd baffle (Figure 2). The experimental setup (Fig. 3b) includes a Leica fluorescence stereomicroscope, 1× Plan Apochromatic common main objective, a custom-built micro image calibration kit, laser and LED illumination, and a checkerboard calibration plate. The selected microscope and objective configuration can produce a stereoscopic half-angle of ~11° in air (full angle 22°), and this means that the uncertainty of the out-of-plane velocity component, w, is expected as 5× that of the in-plane velocity components, u and v (6). Since uncertainty of the in-plane velocity components are on the order or 0.5% (assuming ~0.055 pixels in a 11 pixel displacement in a 32×32 interrogation window) (7), the uncertainty of the out-of-plane velocity component is expected to be on the order or 2,5%.

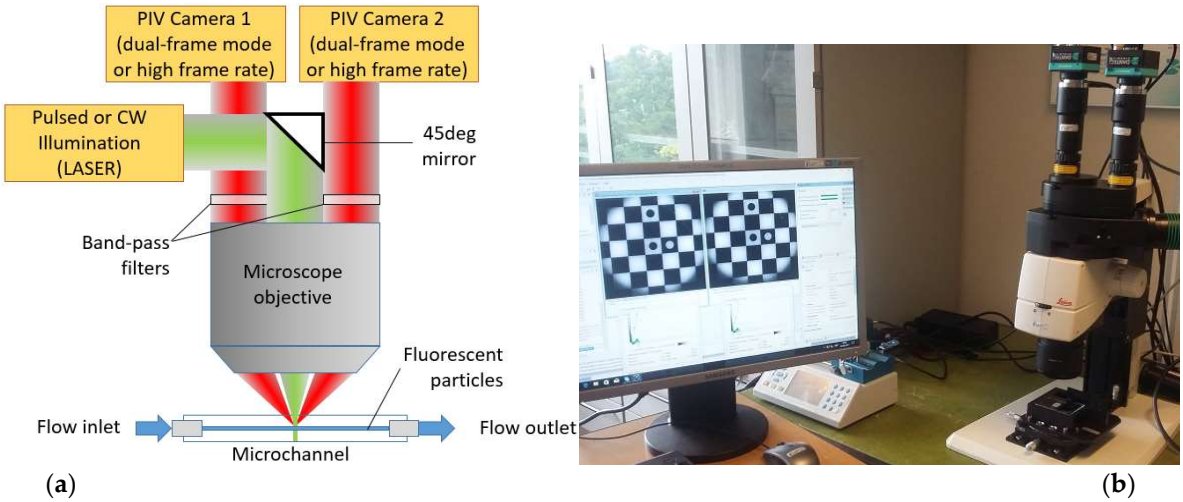

Fig. 3 (a) 2D3CμPIV measurement in back-scatter illumination mode. **(b)** a 2D3CμPIV system featuring a fluorescence stereo microscope, two PIV cameras, a calibration kit and syringe pump.

Stereoscopic image calibration in a microchannel is simply difficult, if not impossible. To achieve an accurate representation of the object space in 3D, a dedicated image calibration kit (Fig. 4a) is used, which consists of a checkerboard calibration target (Fig. 4b), a calibration pool and a micro stage to traverse the target in the calibration pool. The cover glasses of the calibration pool and of the microchannel are the same material (2mm thick glass for the current experiment) simulating similar optical conditions during calibration and measurements. Further details on Stereoscopic MicroPIV measurements can be found in Ref. (8).

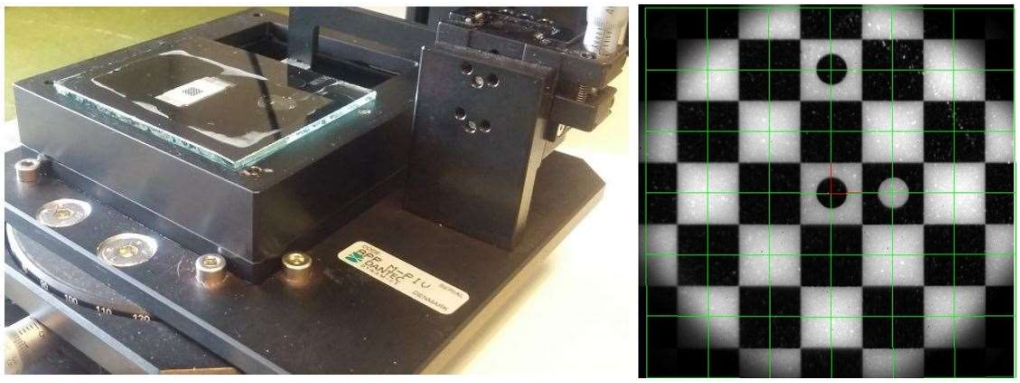

Fig. 4. (a) Stereoscopic image calibration kit for MicroPIV. **(b)** View of the checkerboard calibration target, the coordinate system (red), metric calibration grid (green). Each square edge is 500μm.

The calibration target features a checkerboard pattern for a 4.5 mm object size. Carefully placed three circular markers within the squares allow an unambiguous definition of the planar coordinate axes. During calibration, a pulsed monochromatic LED device is used for illumination, which proves useful in obtaining calibration images with good contrast. The calibration is performed (i) by imaging the checkerboard pattern in known positions within the depth of field (ii) by computing mapping function for the 3D space using a 3rd order polynomial function (9)

and (iii) by performing calibration refinement. The depth of field is controlled by adjusting the aperture of the zoom optics of the stereomicroscope. A depth calibration is also performed for accurate positioning of the measurement plane in the microchannel. The depth calibration, stereoscopic calibration and experiments are performed at 5× total system magnification, which produces a Field of View (FoV) of 3mm × 3mm. During depth calibration and measurements, the aperture was adjusted to produce a 31 μm field depth (important for depth calibration) and 385 μm correlation depth (important for experiments). Five calibration images were used at h= ±200 μm, ±100 μm and 0 μm (center height). The average reprojection error for left and right cameras were found as ~1 pixel because of image calibration using a new marker detection algorithm.

3. Experiments

The flow rig is considerably different from the flow rig used in Ref (2,3), except the flow channel: A water pump and 2 dampers were used in Ref (2,3), and a high precision syringe pump with a linear step resolution of 12 nm is used in this work. Rhodamine B fluorescent particles were used for seeding in both experiments, with 1 μm diameter in in Ref (2,3) and with 1-20 μm-diameter in the current study. The syringe pump's flow rate accuracy and reproducibility are given as ±0.35% and ±0.05% respectively, and therefore no dampers were necessary in the current experiments. The syringe pump can drive two syringes simultaneously and the flow rate is adjustable between 1.6 pl/min to 300 ml/min using different syringe sizes. High quality airtight glass syringes are used to generate a smooth flow during the measurements. Two flow rate settings of 24ml/min and 48ml/min induce Reynolds numbers of 345 and 690 respectively, in order to produce close experimental conditions to those of Ref (2) and (3) where Reynolds numbers were 435, 642 and 867. The flow rates are selected so that they can be compared with the 2D2C PIV results obtained in Ref. (2) and (3). During measurements, pulsed illumination at 532nm from a 50 mJ/pulse dual-cavity Nd:YAG laser is delivered to the microscope using a liquid light guide and imaging is performed using two 12-bit FlowSenseEO 4Mpix (2048pix × 2048pix) PIV cameras. Planar three component velocity measurements are computed by combining the 2D2C velocity field information from each camera, and refined image calibration information. Contrast of raw particle images was enhanced by performing a background subtraction using the minimum pixel value found in the ensemble. An ensemble static masking technique is applied to perform static masking (10), and this static mask was used to improve PIV interrogation near the boundaries (11).

4. Results

Comparison of 2C flow field: we start with some comparisons in the 2D flow field to ensure repeatability of the results. Figures 5 and 6 below shows such comparison for the mean $\bar{u}$ velocity field and mean $\bar{v}$ velocity field, respectively. In Figure 5a and 5b the mean $\bar{u}$ velocity field results of the current study using Stereoscopic MicroPIV system is shown for Re=345 and Re=690, respectively. In Figure 5c, the mean $\bar{u}$ velocity field results for Re=687 from Ref. 1 is shown with similar contour levels to Fig. 5b.

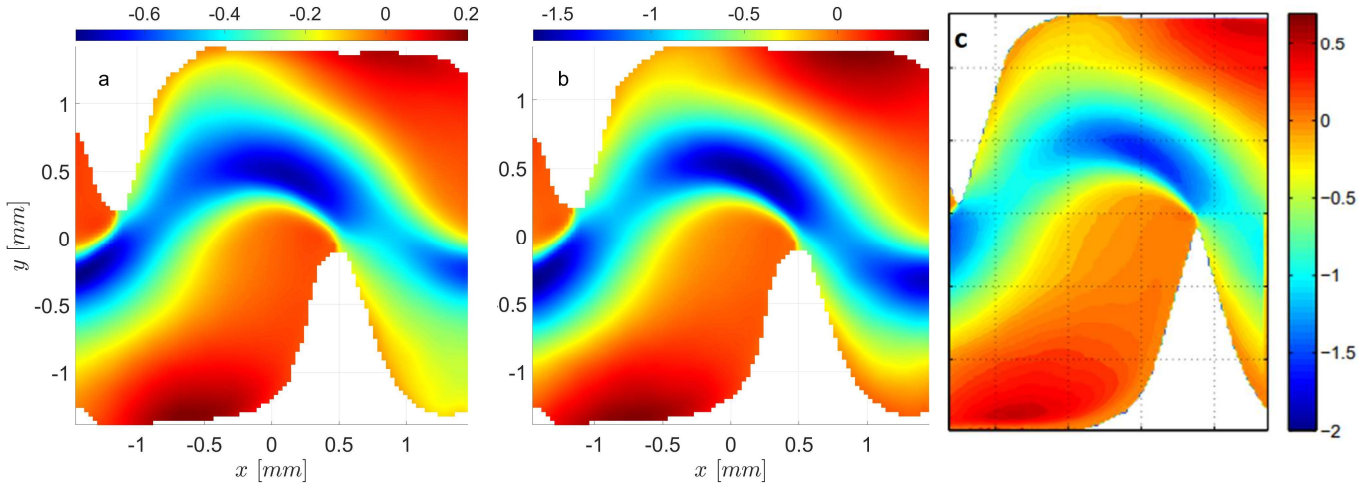

Fig. 5. Mean $\bar{u}$ velocity field (a) Re=345 using Stereo MicroPIV (-0.75 < $\bar{u}$ < 0.25 m/s) N=1000 (b) for Re=690 using Stereo MicroPIV (-1.5 < $\bar{u}$ < 0.5 m/s) N=1000 (c) Re=687 using 2D MicroPIV (-2 < $\bar{u}$ < 0.7 m/s) from Ref. (1) N=500.

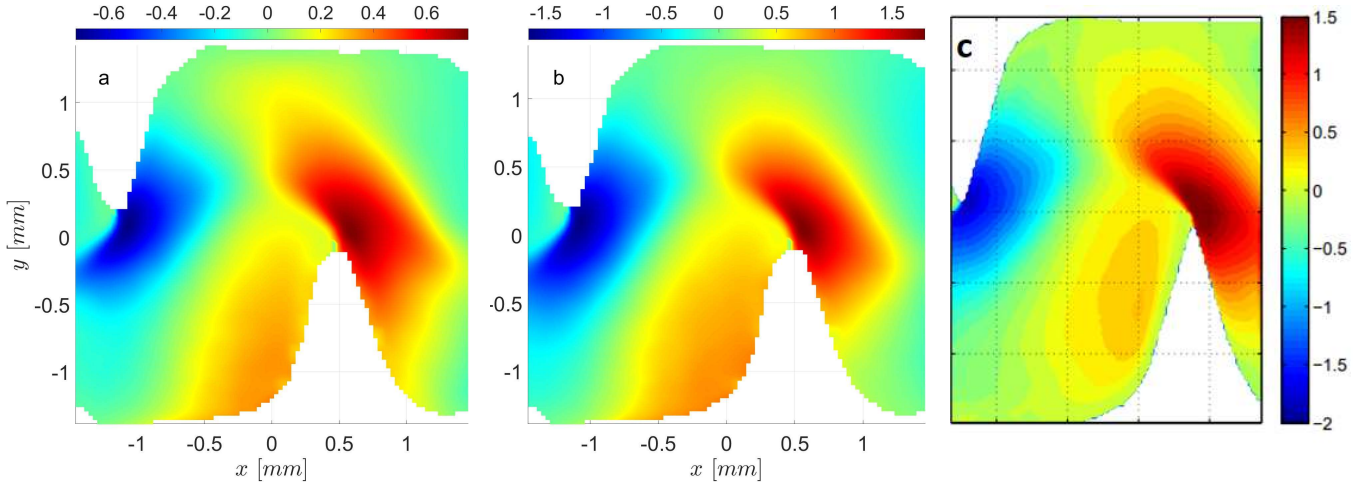

Fig. 6. (a) Mean $\bar{v}$ velocity field (a) for Re=345 using Stereo MicroPIV (-0.75 < $\bar{v}$ < 0.75 m/s) N=1000 (b) Re=690 using Stereo MicroPIV (-1.5 < $\bar{v}$ < 1.5 m/s) N=1000 (c) Re = 687 using 2D MicroPIV (-2 < $\bar{v}$ < 1.5 m/s) from Ref. (1) N=500.

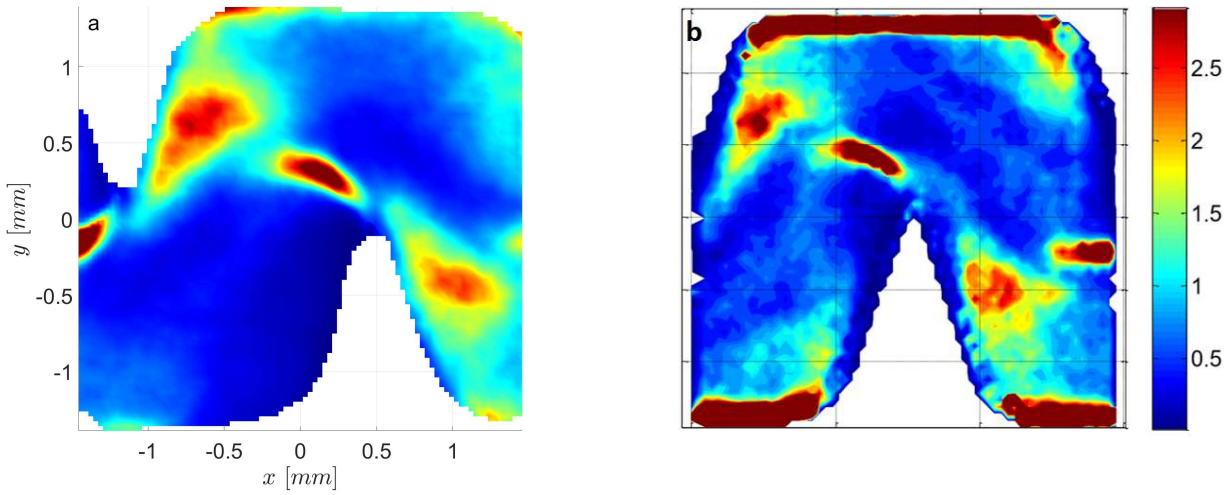

Fig. 7. The $\overline{u'^2}/\overline{v'^2}$ ratio in the third baffle (a) Re=690 using Stereo MicroPIV ($0 < \overline{u'^2}/\overline{v'^2} < 2.8$) N=1000 (b) Re=800 using 2D MicroPIV ($0 < \overline{u'^2}/\overline{v'^2} < 2.8$) from Ref. (12) N=250

Please note that the contour range of Fig. 5a is half of that of Fig. 5b. The three-way comparison suggests that (i) the flow topology is very similar if the mean $\bar{u}$ velocity field is normalized by the Reynolds number, and (ii) the current measurement results using Stereo MicroPIV system have a good agreement with the results obtained using the 2D MicroPIV system. A similar conclusion is reached when the mean $\bar{v}$ velocity field is considered (Fig. 6). It should be noted that the number of images in the ensemble is, N=1000 for the current experiments, and N=500 for the 2D MicroPIV experiments of Ref. (1).

As the mean flow velocity components, $\bar{u}$ and $\bar{v}$ provide a good comparison with the previous results, we attempted to make a comparison of previously reported fluctuating velocity results. Fig. 7 makes such a comparison using the ratio of mean squared velocity components, $\overline{u'^2}/\overline{v'^2}$, in the third baffle. Whereas Fig 7a. shows the $\overline{u'^2}/\overline{v'^2}$ ratio field in the third baffle for Re=690 using Stereo MicroPIV, Fig 7b. shows the same ratio in the same baffle for a slightly higher Re=800 using 2D MicroPIV as reported in Fig. 23 of Ref. (12). Although there is a general good agreement in Fig. 7, there are also noticeable differences. The major difference is the presence of very high values of the $\overline{u'^2}/\overline{v'^2}$ ratio near the top and bottom walls of the channel (Fig 7b). These high values are not visible in the current study (Fig 7a). There can be several reasons why this may be happening, as everything except the flow channel is different in the current study, compared to the rig described in Ref. (12). For example, a pump and 2 damper mechanisms were used in Ref (12), and a precision syringe pump is used in this study. Furthermore, an automated static masking technique is used in this study in combination with interrogation window masking near the walls and these are not used in Ref (12). It is quite possible that the $\overline{u'^2}/\overline{v'^2}$ ratio could yield large values due to undamped oscillations originating from the pump in Ref (12), and these may have gone unnoticed due to lack of wall treatment in data analysis. However, the current study captures the main topology of $\overline{u'^2}/\overline{v'^2}$ field quite well away from the walls. Once again, it should be noted that the number of ensembles is N=1000 for the current experiments, and N=250 for the 2D MicroPIV experiments of Ref (12). All in all, it is quite encouraging that the current Stereo MicroPIV results are in good

agreement with the previously reported 2D MicroPIV results, both in terms of the mean flow and in terms of fluctuating components.

***w* Results**: The mean out-of-plane velocity component, $\overline{w}$ fields for Re=345 and Re=690 cases are shown in Figure 8a and 8b, respectively. The negative values indicate vectors going into the page and the positive values indicate vectors going out of the page. One immediate observation is that the flow topology is very similar if the mean $\overline{w}$ velocity field is normalized by the Reynolds number, as the contour range for Re=345 case is half of the same for Re=690 case. Another observation is that there is a concentration of negative $\overline{w}$ from baffle tips (in purple color), elongated towards the left, in the flow direction. Regions of positive $\overline{w}$ areas (in red colour) parallel to the purple regions may suggest the existence of a vortex tilted ~45° with the x-axis. These locations are marked with black dashed lines in Fig. 8 (1,2,3,4). As mentioned before, serpentine micromixers with sharp turns may induce oblique vortices (4,5), and these can be responsible for enhanced mixing and reduced clogging in the nozzle. To identify such vortices, the 3D view should be used (Fig. 9).

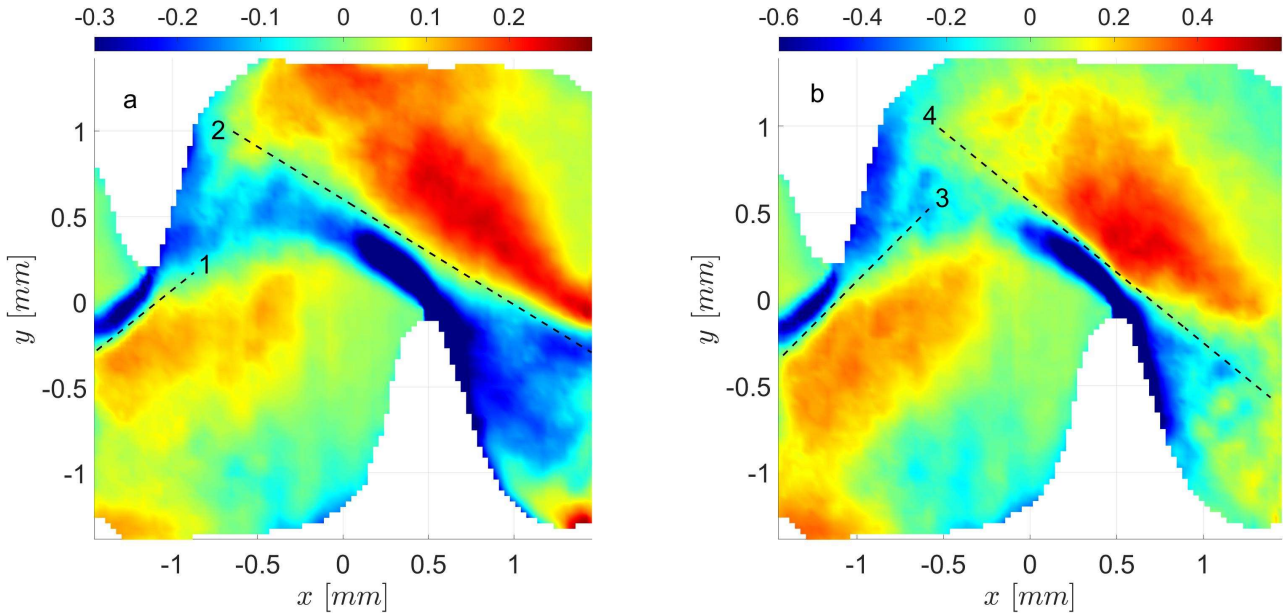

Fig. 8. The mean $\overline{w}$ fields for (a) Re=345 (-0.3 < $\overline{w}$ < 0.3 m/s) and (b) Re=690 (-0.6 < $\overline{w}$ < 0.6 m/s)

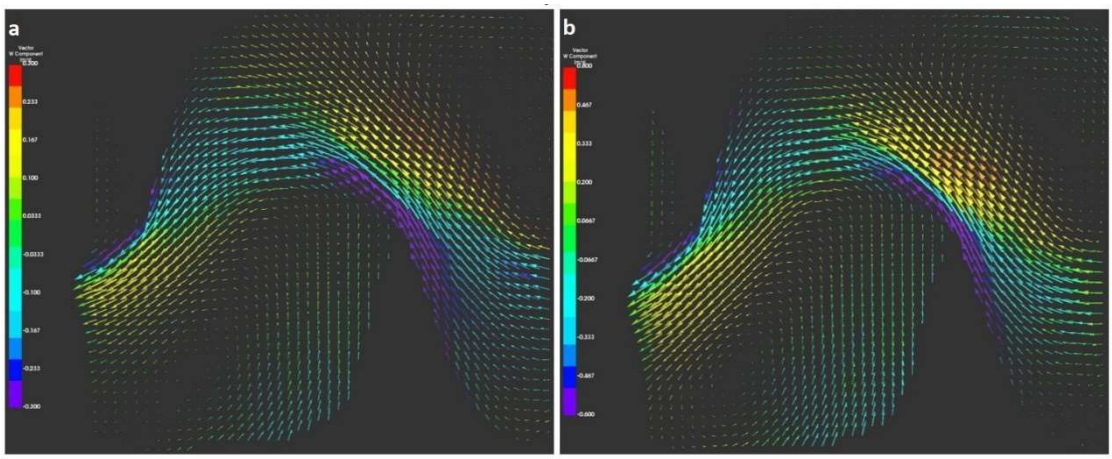

Fig. 9. The mean velocity field, where $\bar{u}$ and $\bar{v}$ are drawn as vectors, and $\bar{w}$ is depicted in colours. (a) Re=345 (-0.3 < $\bar{w}$ < 0.3 m/s) and (b) Re=690 (-0.6 < $\bar{w}$ < 0.6 m/s)

Figure 9 shows the mean velocity field for the experiments, where $\bar{u}$ and $\bar{v}$ are drawn as vectors, and $\bar{w}$ is depicted in colours. The advantage of 3D view is that one can rotate the view freely in any arbitrary axis to visualise potential oblique vortices in the flow field (Figs. 10 and 11). Fig. 10 shows the 3D view for Re=345 case: On the left (Fig 10a) a counter-clockwise (CCW) vortex is identified originating from the baffle on the left in Fig. 8a (dashed line 1), whereas on the right (Fig. 10b) a clockwise (CW) vortex is identified originating from the baffle on the right in Fig. 8a (dashed line 2). Figure 11 shows similar results for the Re=690 case with twice the vortex strength compared to the Re=345 case: On the left (Fig 11a) a counterclockwise (CCW) vortex is identified originating from the baffle on the left in Fig. 8b (dashed line 3), whereas on the right (Fig. 11b) a clockwise (CW) vortex is identified originating from the baffle on the right in Fig. 8b (dashed line 4).

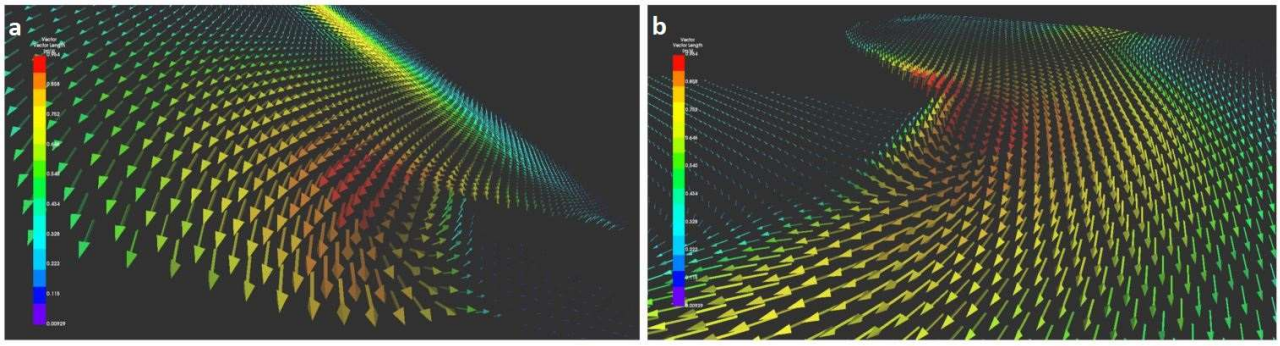

Fig. 10. 3D view for Re=345 (a) CCW vortex on axis 1 in Fig 8a (b) CW vortex on axis 2 in Fig 8a

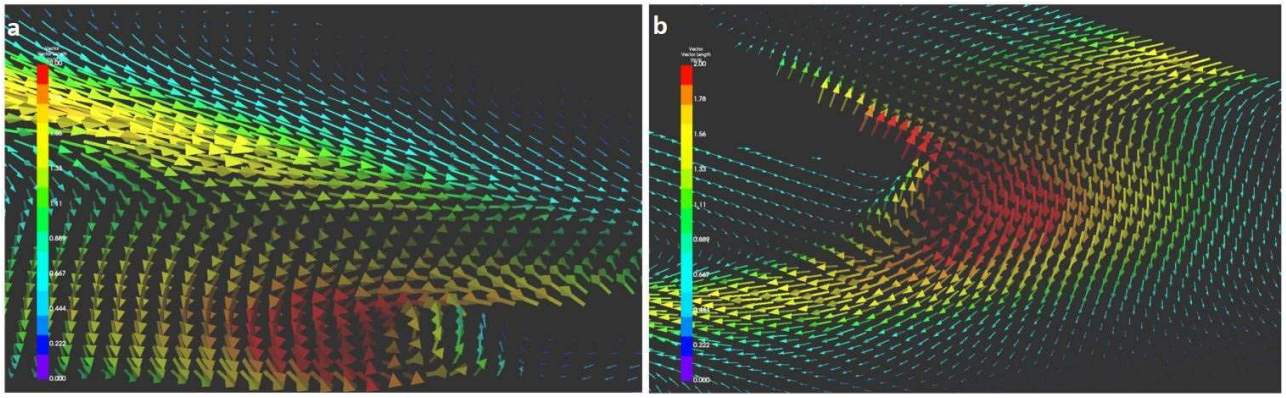

Fig. 11. 3D view for Re=690 (a) CCW vortex on axis 3 in Fig 8b (b) CW vortex on axis 4 in Fig 8b

Mean total velocity: As zero-velocity or low-velocity regions favor sediment deposition which leads to eventual clogging, the mean velocity modulus must be investigated to identify stagnant and recirculation zones in the microchannel. Previous 2D MicroPIV experiments in Ref.s (1–3,12) only measured u and v, so the modulus was computed as $\overline{V_{u,v}} = \sqrt{u^2 + v^2}$, but here it can be computed as $\overline{V_{u,v,w}} = \sqrt{u^2 + v^2 + w^2}$, with the availability of w thanks to the Stereo MicroPIV system. Fig. 12 compares the mean total velocity fields, $\overline{V_{u,v,w}}$, for Re=345 and Re=690 cases for the current study and the $\overline{V_{u,v}}$ from Fig. 12 of Ref. (2) using similar colormaps.

First, a general comparison of current mean total velocity results to previous results shows that the general flow magnitude topology is captured quite well with subtle differences. This is encouraging since we expect the Stereo MicroPIV measurements to have good agreement with the previous 2D MicroPIV experiments, but also reveal new information by the additional measurement of w, which was not available before. Second, we can identify several recirculation and stagnation zones in the microchannel, marked with red and black colors, respectively (Fig. 12a and 12b). These zones are in good agreement with Ref. (2) (Fig. 12c and 12d): The recirculation zones R1 and R2 are slightly larger for the Re=345 case (Fig. 12a), when compared with the Re=690 case (Fig. 12b); and the stagnation zone S1 is smaller for the Re=345 case (Fig. 12a), when compared with S2 in the Re=690 case (Fig. 12b). Finally, a new stagnation zone S3 (Fig. 12b) is visible close to the lower wall only for the Re=690 case and was not visible for the Re=345 case (Fig. 12a). In short, it seems like the recirculation zones are shrinking and stagnation zones expanding with increasing Re number.

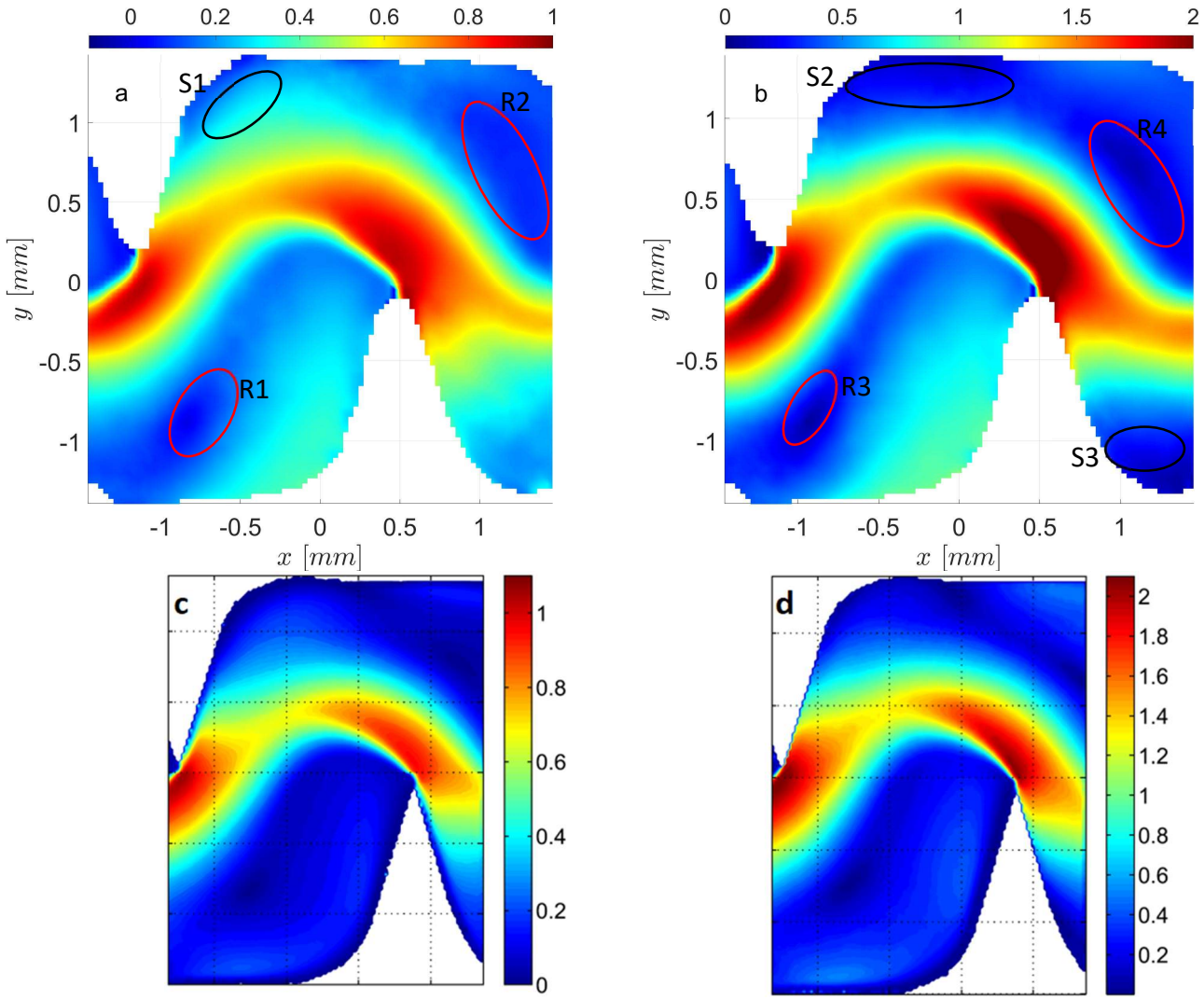

Fig. 12. The mean velocity modulus in the 3rd baffle. (Left) Re=345 (Right) Re=690 (Top) $\overline{V_{u,v,w}}$ of this study (Bottom) $\overline{V_{u,v}}$ from Fig. 12 of Ref. (2). (a and b) Black marks stagnation zones, red marks recirculation zones.

Fluctuating velocity field: The mean $\overline{w}$ fields have shown that an oblique CCW vortex is produced on the lee side of baffles located on the top wall and an oblique CW vortex is produced on the lee side of baffles located on the bottom wall. These vortices could not be observed previously as the out-of-plane velocity component was not measured. Furthermore, the mean total velocity fields show several recirculating and stagnant zones in the microchannel. To draw some conclusions about clogging in the channel, the fluctuating velocity components (Figure 13) should be investigated, together with the mean flow field to check the steadiness of the low- or zero-velocity zones identified earlier in Figure 12.

Figure 13 shows the fluctuating velocity components u' (top row), v' (middle row) and w' (bottom row), for two cases: for Re=345 (left column) and for Re=690 (right column). The contour map ranges for the right column (Re=690 case) are always twice of those on the left column (Re=345

case). This immediately suggests that the components u', v' and w' information scales with Re, as the topology is quite similar on the left and right column within each row. Also marked on Fig. 13 are the stagnation and recirculation zones identified previously in Figure 12a and 12b (marked

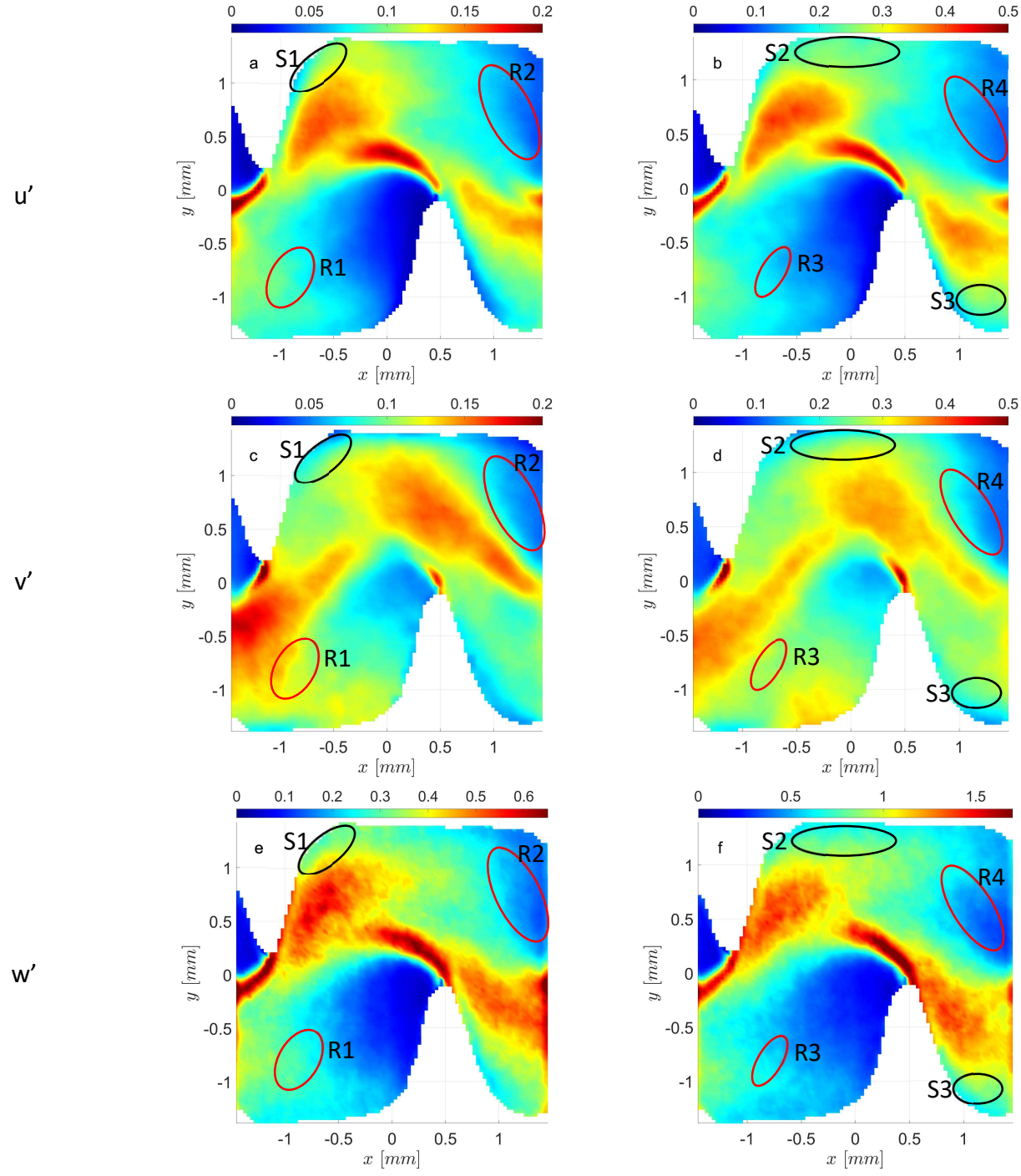

Fig. 13. Fluctuating velocity fields (m/s). (Top) u' (Middle) v' (Bottom) w'. (Left) Re=345 (Right) Re=690. (a) ($0 < u' < 0.135$), (b) ($0 < u' < 0.270$), (c) ($0 < v' < 0.2$) (d) ($0 < v' < 0.4$), (e) ($0 < w' < 0.5$) (f) ($0 < w' < 1$)

again with black and red, respectively). The basic idea is to search for some non-zero values in the fluctuating fields for the low-velocity zones in the mean flow field. If non-zero fluctuating values indeed exist in these zones, this means that the low- or zero-mean-velocity zones suspected of sediment deposition are in fact non-steady, and the particles may not have enough time to settle in these zones. When Fig. 13 is carefully examined in zones R1, R2, R3, R4 and S1, S2, S3; not only the values are non-zero but also they are significantly large within each range. This may explain why the dripper geometry used in the current study and in the previous experiments (1–3,12) is less susceptible for clogging: Using the estimated Kolmogorov time scales from the Reynolds Stress Model numerical simulation of Ref(1) in the range 0.045-0.13 ms for Reynolds numbers between 800 and 400, the Stokes number will be around 0.1 only for sand particles above 10 microns which could begin to be entrapped into the water vortices.

4. Summary and Conclusions

Stereoscopic MicroPIV measurements are performed on a serpentine microchannel geometry which is known to suppress clogging when used in agricultural drip irrigation systems. In short, all 4 aims of this study were fully achieved:

- Comparison of the current three-component (3C) measurements with the 2C measurements in Ref (2), reveals that the flow topology is quite similar, and 3C results are in good agreement with the 2C results, yet adding more information to the existing knowledge on the flow field.
- Oblique vortices emanating from the baffle tips were identified thanks to the measurement of $\overline{w}$ component. These vortices are rotating in CCW and CW directions per baffle, one after the other. These are better visible using 3D viewers, as the flow field in the channel is quite complex. These oblique vortices are very likely to have a contribution to the mixing process in the microchannel and thereby have an influence on clogging suppression.
- The low- and zero-velocity regions, i.e. stagnation and recirculation regions were identified and their steadiness were investigated. It was found that although several stagnation and recirculation zones were identified from the steady flow field results, the unsteady flow fields showed that the fluctuating velocity components are all non-zero.
- Results were evaluated with respect to clogging considering the new information using the Stereo MicroPIV measurements: Following point 3, the fluctuations are thought to be the main contributor for clogging suppression as the particles do not get a chance to settle in these low- and zero-velocity regions due to fluctuations.

The fluctuating $\overline{w}$ fields were observed to have a suspiciously large amplitude and this may be attributed to the larger uncertainty associated with the shallow stereo angle. Another reason could be due to the large correlation depth (385μm) during the experiments. Future work will focus on improving the out-of-plane component accuracy using a thinner correlation depth or using 3D particle tracking in the existing correlation depth. The larger than expected out-of-plane fluctuations do not change the last conclusion above, since the in-plane fluctuations are still non-zero and may be responsible for clogging suppression.

References

1. Al-Muhammad J. Flow in millimetric-channel: numerical and experimental study [Internet]. 2016. Available from: https://tel.archives-ouvertes.fr/tel-01531349
2. Al-Muhammad J, Tomas S, Ait-Mouheb N, Amielh M, Anselmet F. Micro-PIV characterization of the flow in a milli-labyrinth-channel used in drip irrigation. Exp Fluids [Internet]. 2018 Dec 9;59(12):181. Available from: http://link.springer.com/10.1007/s00348-018-2633-x
3. Al-Muhammad J, Tomas S, Ait-Mouheb N, Amielh M, Anselmet F. Experimental and numerical characterization of the vortex zones along a labyrinth milli-channel used in drip irrigation. Int J Heat Fluid Flow [Internet]. 2019 Dec;80:108500. Available from: https://linkinghub.elsevier.com/retrieve/pii/S0142727X19300104
4. Ergin FG. Velocity measurements in an Omega-micromixer using Stereo-MicroPIV. In: Proc 5th Micro and Nano Flows Conference Milan, Italy, 11-14 September 2016. 2016.
5. Ergin FG, Tomas S, Pătraşcu C. Stereo MicroPIV measurements in an irrigation nozzle. In: E3S Web of Conferences. 2019.
6. Prasad AK. Stereoscopic particle image velocimetry. Exp Fluids. 2000;29(2):103–16.
7. Ergin FG, Watz BB, Erglis K, Cēbers A. Time-resolved velocity measurements in a magnetic micromixer. Exp Therm Fluid Sci. 2015;67:6–13.
8. Ergin F, Watz B, Gade-Nielsen N. A Review of Planar PIV Systems and Image Processing Tools for Lab-On-Chip Microfluidics. Sensors [Internet]. 2018;18(9):3090. Available from: http://www.mdpi.com/1424-8220/18/9/3090
9. Soloff SM, Adrian RJ, Liu Z-C. Distortion compensation for generalized stereoscopic particle image velocimetry. Meas Sci Technol [Internet]. 1997 Dec 1;8(12):1441–54. Available from: https://iopscience.iop.org/article/10.1088/0957-0233/8/12/008
10. Ergin FG. An automatic static masking technique using Particle Image Velocimetry image ensembles. Exp Therm Fluid Sci [Internet]. 2021 Oct;128:110431. Available from: https://linkinghub.elsevier.com/retrieve/pii/S0894177721000807
11. Ergin FG. PIV accuracy improvement near stationary walls using interrogation window masking. In: Proc 12th Int Symp on Particle Image Velocimetery, Pusan, Korea. 2017.
12. Al Muhammad J, Tomas S, Mouheb NA, Amielh M, Anselmet F. μ-PIV characterization of the flow in a milli-labyrinth-channel used in micro-irrigation. In: 17th International Symposium on Applications of Laser Techniques to Fluid Mechanics. 2014. p. 15.